An Effective Chatter Detection Method in Milling Process Using Morphological Empirical Wavelet Transform

Qi Zhang, Xiaotong Tu, Fucai Li, and Yue Hu

***Abstract*— The empirical wavelet transform (EWT) has shown its effectiveness in some applications. However, when noisy and nonstationary signals are analyzed, some local maxima may appear and be retained in the peak sequence mistakenly, so improper segmentation in the frequency domain will occur. In our research, the morphological EWT (MEWT) method is proposed based on morphological filters (MFs) and the 1-D Otsu method to mitigate the boundary segmentation drawback of the EWT, and it can be applied in chatter detection because of its good performance in finding the optimal chatter frequency band. First, the local maxima distribution plane is calculated using MFs. Then, the 1-D Otsu method processes the distribution plane and then achieves the optimal threshold for MFs. For MEWT's better application in chatter detection, an automatic selection of the parameter *K* using kurtosis is proposed and it breaks away from the previous empirical selection. Finally, since it is known that energy will transfer to chatter frequency bands when chatter occurs in the milling, the energy entropy of each subsignal used is to detect chatter frequency bands and choose the optimal chatter monitor indicator. The relevant simulation and experimental signals have been analyzed for verifying the validity of the MEWT and the novel chatter detection method with strong sensitivity to chatter.**

***Index Terms*— Chatter detection, fault diagnosis, morphological empirical wavelet transform (MEWT), optimal chatter indicator.**

I. Introduction

CHATTER is one of the harmful influencing factors affecting the performance of machining operations, and it stems from the self-excited vibration. When this system is activated by the cutting force, it causes chatter, and chatter frequencies are close to the natural frequency of the system [1]. Chatter usually affects the surface quality and the production efficiency and causes tool wear [2], [3]. Moreover, chatter will increase the rejection rate in mass production, causing huge economic losses. So, many researchers have proposed many approaches which contain chatter stability prediction [4], chatter detection [5], and chatter suppression [6].

Because of the intelligence of the chatter detection method, it is significant to realize high efficiency and precision machining. However, chatter stability analysis is difficult to be used efficiently in the practical milling process. By contrast, chatter detection can help the machine to evade chatter at the early stage. In recent years, signal processing methods of chatter detection have been widely developed, as seen in [7] and [8].

In chatter detection, extracting features is the core step. But the first step is to select a suitable signal before the extraction. Different signals have been selected to monitor chatter, such as the cutting force [9]–[11], acceleration signals [12], [13], motor currents [14], [15], sound signals [16]–[18], torque signals [19], and vibration signals [20]–[23]. Gindy *et al.* [24] proposed that vibration signals are more sensitive in detecting chatter than cutting force signals. Kuljanic *et al.* [25] developed a sensor-based acceleration signal detection system.

Whatever signal is used to detect the chatter, frequency bands including chatter information should be identified efficiently before running its detection. Signal processing plays a significant role in finding out chatter frequency bands. Amezquita-Sanchez *et al.* [26] described a review of the latest research works on vibration-based signal processing technology for structural health monitoring. Nowadays, those methods in different domains (time; frequency; time–frequency) have been used to extract features. Specifically, these methods in the time–frequency domain have been employed for locating the time and the frequency [27], [28], such as short time Fourier transform (STFT), ensemble empirical mode decomposition (EEMD), wavelet packet transform (WPT), and empirical wavelet transform (EWT) [29]–[33]. Cao *et al.* [27] utilized EEMD to analyze vibration signals, then the C_0 complexity and the power spectrum entropy were extracted as indicators to detect chatter; EWT has been used to verify the fault information on rolling bearings [34]; Jauregui-correa *et al.* [12] proposed the method using detrended fluctuation analysis to detect chatter.

In addition, the energy distribution in each frequency band is different and it will change under different milling conditions [27]. It is suitable to use energy entropy to represent cutting conditions. For instance, energy entropy was applied to identify roller-bearing faults by Yu *et al.* [21]. Zhang *et al*. [31] proposed a method to detect chatter based on the energy entropy of VMD and WPT; however, its sensitivity

Manuscript received September 11, 2019; revised October 19, 2019; accepted November 29, 2019. Date of publication December 9, 2019; date of current version June 24, 2020. This work was supported by the National Major Science and Technology Project of China under Grant 2017ZX04011014. The Associate Editor coordinating the review process was Dr. Loredana Cristaldi. *(Corresponding author: Fucai Li.)*

The authors are with the State Key Laboratory of Mechanical System and Vibration, Shanghai Jiao Tong University, Shanghai 200240, China (e-mail: qizhang@sjtu.edu.cn; tormii@sjtu.edu.cn; fcli@sjtu.edu.cn; huyue_sjtu@sjtu.edu.cn).

Color versions of one or more of the figures in this article are available online at http://ieeexplore.ieee.org.

Digital Object Identifier 10.1109/TIM.2019.2958470

is not good because of the analysis of the overall signal. Since it calculates the energy entropy of the overall signal, when chatter occurs, the rate of energy entropy change from stable milling to slight chatter is only 2.42%, which is not sensitive to the occurrence of chatter. So, it severely restricts its practical application in engineering. Liu *et al.* [32] used the VMD to detect chatter, but the relevant operation of the parameter K and α of VMD consumes plenty of time, which cannot be applied in the practical milling process. Therefore, the results of the above methods show that energy entropy could identify chatter, but its sensitivity becomes the focus. Otherwise, finding the chatter frequency bands is the most important step; however, EWT has drawbacks to segment the spectrum. When analyzing noisy and nonstationary signals, some local maxima generated by noise and nonstationary components may appear and be mistakenly retained in the peak sequence, which results in improper segmentation. Whether it has a reasonable spectrum segmentation or not affects the selection of later chatter frequency bands. Hence, segmentation is our first focus.

First, a better boundary division approach is proposed to mitigate the drawback of EWT in segmentation. In MEWT, 1-D Otsu processes the local maxima distribution plane of MFs to calculate a filter's optimal threshold, which is helpful to save useful dominant frequency peaks. Besides, although the proposed MEWT is used in chatter detection, it can be used in roll-bearing fault diagnosis due to its better segmentation property.

Then, the chatter detection method includes an automatic selection of decomposition number K with maximum kurtosis, which will determine the input parameter of MEWT. After decomposition, the energy entropy theory helps select the optimal chatter indicator by comparing its change under three milling conditions. Moreover, because of its good computational speed, the indicator can be utilized in practical milling systems with excellent sensitivity about whether chatter occurs.

Other sections are constituted as follows. Section II explains the theoretical background of EWT and energy entropy. Section III describes the MEWT utilizing MFs and 1-D Otsu. Section IV describes the chatter detection based on the proposed MEWT. In Section V, the simulation signal is used to prove the validity of the above chatter detection method. Section VI describes the relevant experiment and discussion of results obtained from the chatter detection method. Section VII describes some conclusions of this article.

II. Theoretical Background

A. EWT Method

EWT is a method employed to extract instantaneous frequencies of a time series signal. The core step in the EWT process is the segmentation of the Fourier spectrum, and another step is used to construct empirical wavelets and apply them to process segments. In order to segment a signal's Fourier spectrum, the first thing is to estimate the local maxima of the spectrum. After that, the center between two consecutive maxima is defined as the boundaries of all segmentations.

Additionally, N contiguous segments are related to a range of $0 \sim \pi$ in the spectrum. The frequency band of each segment is defined as $S_n = [\omega_{n-1}, \omega_n]$ (where $\omega_0 = 0$ and $\omega_N = \pi$) and $\bigcup_{n=1}^{N} S_n = [0, \pi]$, and a transient phase with its width about $2\tau_n$ is defined around each ω_n. Besides, a specific explanation about how to select τ_n can be learnt from Gilles [30].

The basic function used in EWT is the Meyer wavelet. The corresponding scaling functions are defined by Gilles as

$$\phi_n(\omega) = \begin{cases} 1, & \text{if } |\omega| \le \omega_n - \tau_n \\ \cos\left[\frac{\pi}{2}\beta\left(\frac{1}{2\tau_n}(|\omega| - \omega_n + \tau_n)\right)\right], & \\ & \text{if } \omega_n - \tau_n \le |\omega| \le \omega_n + \tau_n \\ 0, & \text{otherwise.} \end{cases} \tag{1}$$

Besides, the empirical wavelet functions are defined as

$$\psi_n(\omega) = \begin{cases} 1, & \text{if } \omega_n + \tau_n \le |\omega| \le \omega_{n+1} - \tau_{n+1} \\ \cos\left[\frac{\pi}{2}\beta\left(\frac{1}{2\tau_{n+1}}(|\omega| - \omega_{n+1} + \tau_{n+1})\right)\right], & \\ & \text{if } \omega_{n+1} - \tau_{n+1} \le |\omega| \le \omega_{n+1} + \tau_{n+1} \\ \sin\left[\frac{\pi}{2}\beta\left(\frac{1}{2\tau_n}(|\omega| - \omega_n + \tau_n)\right)\right], & \\ & \text{if } \omega_n + \tau_n \le |\omega| \le \omega_n + \tau_n \\ 0, & \text{otherwise} \end{cases} \tag{2}$$

where $\beta(x)$ is the polynomial function, which has the following property:

$$\beta(x) = \begin{cases} 0, & \text{if } x \le 0 \text{ and } \beta(x) + \beta(1-x) = 1 x \in [0, 1] \\ 1, & \text{if } x \ge 1. \end{cases} \tag{3}$$

One low-pass $\emptyset_n(\omega)$ and $N - 1$ bandpass $\varphi_n(\omega)$ filters correspond to the approximation and details, respectively, for each frequency. There is so many polynomial functions satisfying the above properties. So, the auxiliary function suggested by Daubechies is also used in this article

$$\beta(x) = x^4(35 - 85x + 70x^2 - 20x^3). \tag{4}$$

With wavelet filters built above [see (1) and (2)], the time series signal can be decomposed into several frequency bands by using EWT, defined as

$$W_f^{\varepsilon}(0, t) = F^{-1}(x(\omega)\varphi(\omega)) \tag{5}$$

$$W_f^{\varepsilon}(n, t) = F^{-1}(x(\omega)\psi(\omega)) \tag{6}$$

where F^{-1} presents the inverse Fourier transform, and the coefficients of approximation and details are denoted $W_f^{\varepsilon}(0, t)$ and $W_f^{\varepsilon}(n, t)$, respectively. They are the inner products calculated by the signal with the empirical wavelets' low-pass and bandpass filters, respectively.

The method mentioned above is effective in processing signals with better frequency separation. However, it has some drawbacks limiting its application. For example, the peak sequence would mistakenly include some local maxima caused by noise and nonstationary components, and some useful local maxima will not remain in the peak sequence, which will result

in improper segmentation. In addition, using the scale space representation for EWT would result in several subsignals presenting the same characteristics [35].

Due to the practical characteristics of chatter having nonlinear and nonstationary phenomena in the milling process [31], EWT should be enhanced in the segmentation to enable it to be applied in chatter detection better.

B. Energy Entropy Theory

Entropy is a method to illustrate the confusion degree of the system. Energy entropy is an expansion of entropy in the energy domain. The modes obtained from MEWT show a set of subsignals, $p_1(t), p_2(t), \ldots, p_N(t)$, and they represent different frequency bands from low to high frequency. Each subsignal contains the corresponding energy, which can be calculated as

$$E_i = \int_{-\infty}^{+\infty} |p_i(t)|^2 dt, \quad i = 1, 2, \ldots, N \tag{7}$$

where E_i represents the energy of modes.

For convenience, the energy values calculated above are normalized by

$$\varepsilon_i = \frac{E_i}{E_{\text{sum}}} \tag{8}$$

where $E_{\text{sum}} = E_1 + E_2 + \cdots + E_N$. Energy entropies are calculated based on Shannon's entropy as

$$EE_i = -\varepsilon_i \ln \varepsilon_i. \tag{9}$$

Furthermore, energy distributions change in different cutting conditions. In the stable, rotation frequency and harmonic frequencies dominate the energy; when it occurs chatter, the energy distribution of the milling system will transfer to chatter frequencies obviously. Therefore, there is a closer relationship between the energy distribution and cutting conditions, and it can be used to detect whether chatter exists in the milling.

III. MEWT

To change the improper segmentation in EWT, MEWT is devised in our research, which considers the spectrum to detect the better boundaries. It utilizes MFs to find dominant peaks and uses 1-D Otsu to find out the optimal threshold which helps MFs pick out useful peaks. The specific procedure of the MEWT is as follows.

1) Obtain the frequency spectrum of the raw signal using the fast Fourier transform algorithm (FFT).
2) Obtain the local maxima distribution plane of the frequency spectrum based on the MFs.
3) 1-D Otsu method is utilized to calculate the maxima distribution plane and obtain the optimal threshold of the structure element (SE).
4) Detect spectrum boundaries and then divide the spectrum.
5) Decompose the raw signal into several components.

The flowcharts of MEWT and EWT are shown in Fig. 1. The improved method is marked with dotted lines. Then, the MF basis and how to find out the optimal threshold of SE are discussed.

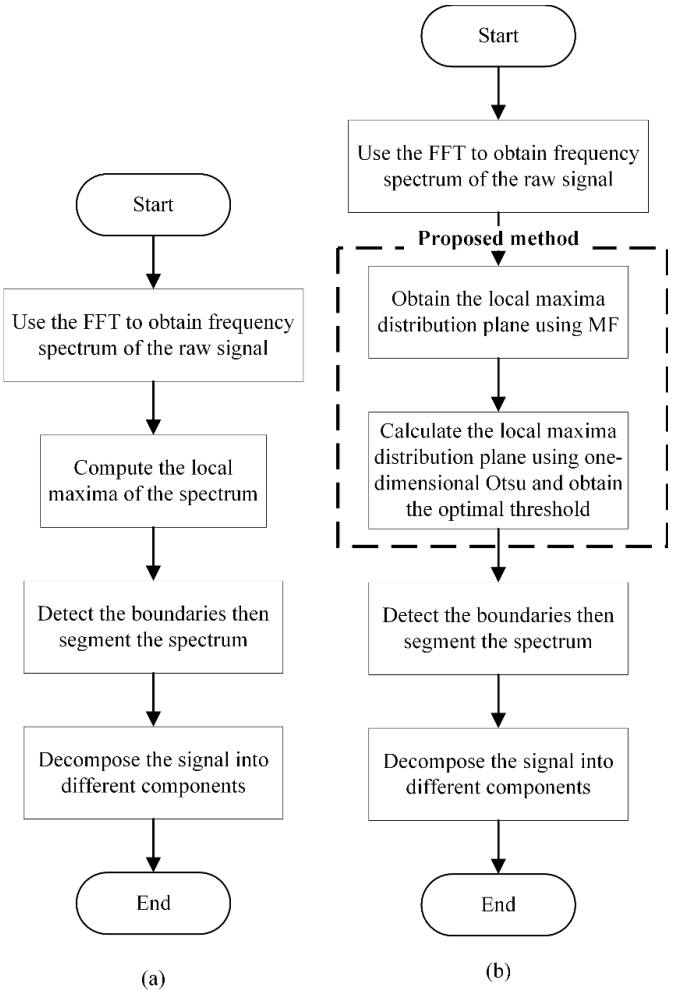

Fig. 1. Flowcharts of (a) EWT and (b) MEWT.

A. Theory of the MF

Mathematical morphology is originally used for image processing. Subsequently, it has been used in digital signal processing, which is to investigate the relationship between signal and the features by using a "probe" SE. In this process, the SE plays an important role in matching the raw signal, maintaining the details, and reducing the noise.

First, the morphological operators include four basic types, such as dilation, erosion, opening, and closing, and the dilation filter is chosen to process the signal. Additionally, it is known that it has the ability to reduce the noise and extract these useful features. The function of the dilation operator is defined as

$$(f \oplus g)(n) = \max[f(n-m) + g(m)] \tag{10}$$

where $\oplus$ represents the dilation operator, $f(n)$ is the analyzed signal, and $g(m)$ is the SE whose length is M. What is more, SE has many types, such as flat, semicircular, and triangular. In this article, the flat SE is applied for its advanced denoising ability and lower computing costs.

After using the dilation operator, the local maxima in the spectrum can be found out. The length of SE has a relationship

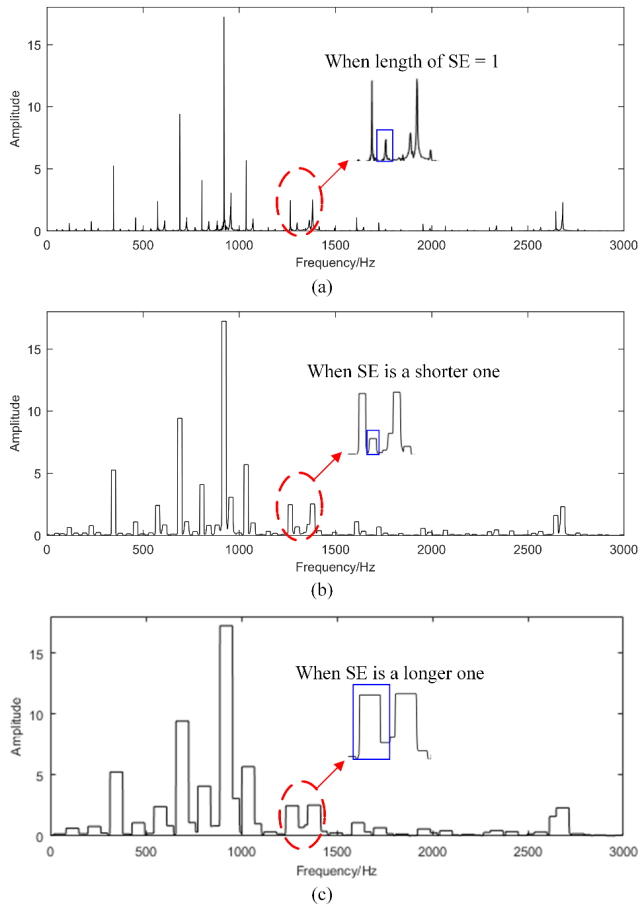

Fig. 2. Signal spectrum (a) with the length of SE = 1, (b) with a shorter SE, and (c) with a longer SE.

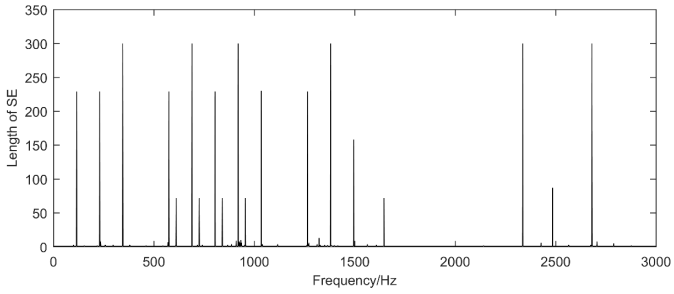

Fig. 3. Local maxima distribution plane of the spectrum of the signal.

with the number of local maxima. Fig. 2 shows an example to illustrate the relationship. To be specific, the local maxima selected by the blue lines disappeared with increasing length of SE, which represents the importance of an appropriate length.

However, because the length of SE is fixed, the dilation operator can only process single-scale analysis, and it is hard to select an appropriate length of SE. Sometimes, some important features will be lost because of this drawback. In order to mitigate the weakness, SEs of different lengths are used to process the spectrum of the signal. The calculated local maxima are drawn in Fig. 3, and they are called the maxima distribution plane.

In Fig. 3, some maxima always exist with the increasing length of SE. When the length of SE is 1, all local maxima are shown in the plane. The lengths of SEs of all maxima are defined as $\mathrm{Ind}_i (i \in [1, n])$, while n is the number of initial maxima, when the length of SE $= 1$.

However, with the increase of SE's length, some maxima will disappear from the plane, which can help judge the consistency of the corresponding maxima, and a bigger length means that the maxima have more possibilities to be the dominant peak.

Therefore, a threshold should be obtained to select the useful maxima, the length of which is bigger than the threshold.

B. Optimal Threshold of MF Based on 1-D Otsu

The Otsu method was proposed by Nobuyuki Otsu [36]. This method is employed to search for the threshold that minimizes the intraclass variance and has been employed in picture processing, such as histograms. Otsu said that minimizing the intraclass variance was similar to maximizing the interclass variance, which is defined as

$$\begin{aligned}\sigma_b^2(t) &= \sigma^2 - \sigma_\omega^2(t) = \omega_0(\mu_0 - \mu_T)^2 + \omega_1(\mu_1 - \mu_T)^2 \\ &= \omega_0(t)\omega_1(t)[\mu_0(t) - \mu_1)(t)]^2 \end{aligned} \tag{11}$$

where ω and μ represent the class probability and the class mean, respectively.

In addition, the class mean can be calculated as

$$\begin{cases} \mu_0(t) = \dfrac{\sum_{i=0}^{t-1} ip(i)}{\omega_0(t)} \\ \mu_1(t) = \dfrac{\sum_{i=t}^{L-1} ip(i)}{\omega_1(t)} \\ \mu_T(t) = \sum\limits_{i=0}^{L-1} ip(i) \end{cases} \tag{12}$$

Otherwise, the class probability can be calculated as

$$\begin{cases} \omega_0(t) = \sum\limits_{i=0}^{t-1} p(i) \\ \omega_1(t) = \sum\limits_{i=t}^{L-1} p(i) \end{cases} \tag{13}$$

where L shows the bins of the histogram.

In this article, 1-D Otsu is utilized to optimize the threshold. The aim is to find an optimal threshold maximizing the interclass variance of the two classes. By using the Otsu to process the distribution plane, the optimal threshold is gained. With the optimal threshold, the dominant peaks are selected, which helps the later boundary detection.

The procedure of 1-D Otsu is shown in Table I. The parameter Ind is the length of SE of the different frequency f in the distribution plane, $p[i]$ represents the ratio of the SE, ω_1 and ω_2 represent the probabilities of class, μ_1 and μ_2 represent the class mean, and ϑ is the variance between classes. In this algorithm, all ϑ are calculated, and the biggest ϑ is selected and the corresponding threshold is the optimal SE, which will be used to help MF find out the dominant peaks.

TABLE I
PSEUDO-CODE FOR ALGORITHM 1

Algorithm 1: One dimensional Otsu

Initialization: ω_1、 ω_2、 μ_1、 $\mu_2 \leftarrow 0$.
N ← length(Ind[*f*]).
for i ← 1 **to max**(Ind)
  f[i] ← length(find(Ind==i)).
  p[i] ← f[i]/N.
end for
for t ← 1 **to max**(Ind)
  for i ← 1 **to** t
    ω_1=ω_1+p[i].
    μ_1=μ_1+i×p[i]/ ω_1.
  end for
  ω_2=1-ω_1.
  for i ← t+1 **to max**(Ind)
    μ_2=μ_2+i×p[i]/ ω_2.
  end for
  $\mu_t = \omega_1 \times \mu_1 + \omega_2 \times \mu_2$.
  $\vartheta[t] = \omega_1 \times (\mu_1 - \mu_t)^2 + \omega_2 \times (\mu_2 - \mu_t)^2$.
end for
optimal threshold: Ind ← **max**(ϑ[t]).

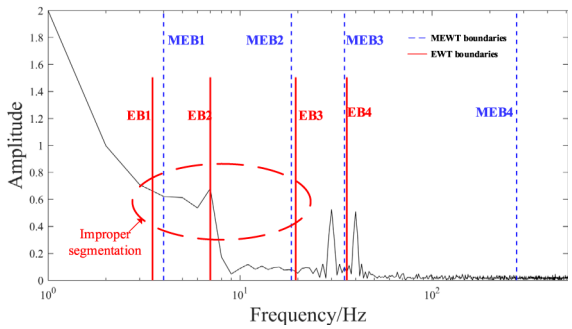

Fig. 4. Spectrum of a simulation signal and its boundaries under two methods.

After finishing the above process, the middle points between the consecutive dominant peaks are defined as the boundaries. Every boundary is the average value between consecutive useful peaks in the spectral domain. If boundaries are expressed as B_n and the dominant peaks are expressed as UP_n, then

$$B_n = \begin{cases} \dfrac{UP_n + UP_{n+1}}{2}, 1 \le n \le K-2 \\ \dfrac{UP_n + \frac{f_s}{2}}{2}, n = K-1 \end{cases} \tag{14}$$

where K is the number of dominant peaks. Finally, B_n will help to decompose a signal into several modes.

Finally, MEWT is designed with the above theories. By analyzing the simulation signals, the effectiveness of MEWT has been verified. In Fig. 4, the boundaries of a nonstationary signal when using EWT and MEWT are shown. As is seen, boundaries of MEWT are more reasonable than those of EWT. For example, EWT cannot separate the high frequency from noise. By contrast, MEWT has the ability to separate the noise because of the fourth boundary (MEB4). EB1 and EB2 in EWT resulted from improper segmentation, while MEB1 replaces the two improper boundaries.

IV. APPLICATION OF MEWT IN CHATTER DETECTION

A. Automatic Determination of the Optimal Parameter K

The parameter K plays an important role in decomposing the raw signal when using MEWT. In the past, it was chosen empirically. So, using the kurtosis to confirm the parameter K is proposed.

Kurtosis is a numerical statistic reflecting distribution characteristics of random variables, and it is the normalized fourth-order central moment. The kurtosis of the reconstruction signal can be calculated by using the following equation:

$$Y = \frac{1}{N}\sum_{i=1}^{N}\left(\frac{x_i - \bar{x}}{\sigma_i}\right)^4 \tag{15}$$

where x_i represents data, $\bar{x}$ represents the mean of data sequence, N is the length of the signal, and σ_i is the its standard variance. When a system has chatter, the signal amplitude increases and the signal deviates from the normal distribution, leading to the increase of kurtosis. Therefore, kurtosis is used as the index of MEWT parameter selection.

1) The limit value δ is set. The minimum energy ratio η_i of all subsignals should be above δ, which will help find out the maximal possible $K_{\max}$. Besides, δ cannot be too large, because it will lead to a wider frequency band and stack too much frequencies in one same band. Therefore, we consider setting it as small as possible and making the maximum possible number of decomposition K as large as possible. By processing the simulation signal, we find that the energy ration of the Gaussian white noise band without obvious peaks is close to 0.07%. Finally, δ chose a smaller value than that and is set as 0.05% based on that simulation.
2) The scope of K is set to $[1, K_{\max}]$ and the step of K is set to T_K. So, the number of all possible K is $((K_{\max} - 1)/(T_K + 1))$.
3) The raw signal is decomposed by the MEWT under all groups K. Then, the raw signal is decomposed into K subsignals. Then, the reconstructed signal is obtained from sub-signals. The maximum kurtosis of all reconstructed signals can be found and the K can be recorded as the best one. Finally, the subsignals of chatter feature extraction are obtained.

B. Establishment of Chatter Detection Method

After that, the chatter detection method can be built based on MEWT. The detection method is shown in Fig. 5. First, in order to automatically choose MEWT's optimal parameter K, a mathematical statistic value, kurtosis, is chosen to find the best K. Then, the proposed MEWT is utilized to decompose the raw signal and obtain some subsignals. Finally, the energy entropy method is used to analyze these subsignals and then select a suitable chatter feature indicator.

V. ANALYSIS OF THE SIMULATION SIGNAL

A. Simulation Signal and Its FFT

In order to prove the validity of the proposed method, a simulation signal [32] is analyzed first. This signal which

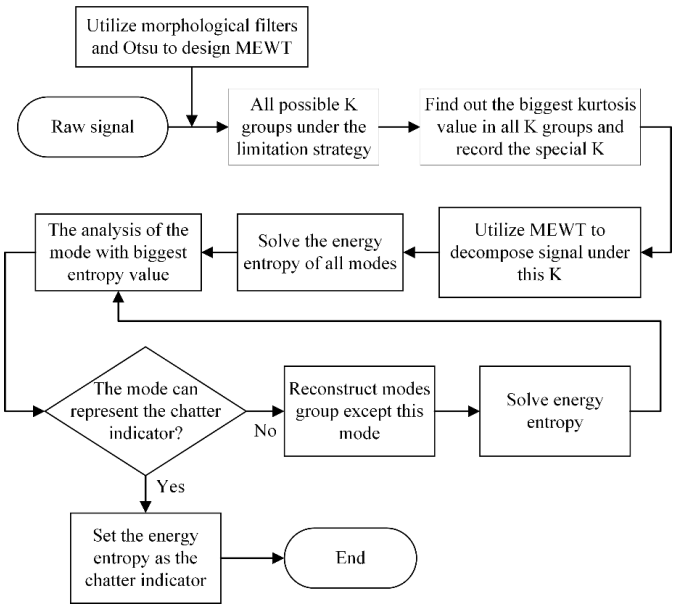

Fig. 5. Flowchart of the proposed chatter detection method based on MEWT.

contains abundant chatter frequencies is defined by (16). This simulation signal includes four different components: 1) stable component x_1 with the low frequency, which is $\omega_1 = 20$ Hz; 2) stable component x_2 with the high frequency, which is $\omega_2 = 80$ Hz; 3) the coupling frequency component x_3, which includes the coupling of the amplitude and the phase to simulate chatter frequencies; and 4) x_4 is the white noise component

$$x(t) = x_1(t) + x_2(t) + x_3(t) + x_4(t) \tag{16}$$

where

$$x_1(t) = 5\cos(40 \times \pi \times t), \quad x_2(t) = 4\sin(160 \times \pi \times t)$$
$$x_3(t) = 0.5(1 + 0.6\sin(30 \times \pi \times t)) \times \cos(300 \times \pi \times t + 1.5\sin(15 \times \pi \times t)).$$

In order to know specific frequency information on x(t), this signal can be processed by using FFT, and its result is shown in Fig. 8(a). As is seen, the frequency band [100 Hz, 200 Hz] includes the chatter frequencies. Those chatter frequencies are a(120 Hz), b(128 Hz), c(135 Hz), d(143 Hz), m(150 Hz), e(157 Hz), f(165 Hz), g(172 Hz), and h(180 Hz).

B. Selection of the Optimal Parameter K for MEWT Based on Kurtosis

To fully consider the impact of K on MEWT, the limit value δ is set to 0.05% empirically and $K_{\max} = 8$ is calculated with δ. The step of K, T_K, is set to 1. After that, the 2-D graph of kurtosis can be drawn, and is shown in Fig. 6.

It is clear that the maximum is 2.2221, when $K = 8$. The maximum possible $K = 8$ is obtained under the empirical limit value δ. In addition, this article does not analyze the impact rule of this statistic, since the magnitude of kurtosis can fully reflect the degree of chatter. Then, the raw signal will be decomposed into subsignals by using MEWT with this K.

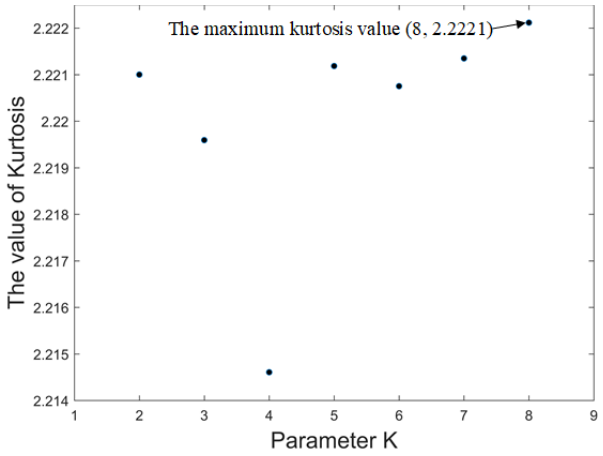

Fig. 6. 2-D graph of kurtosis under all possible K.

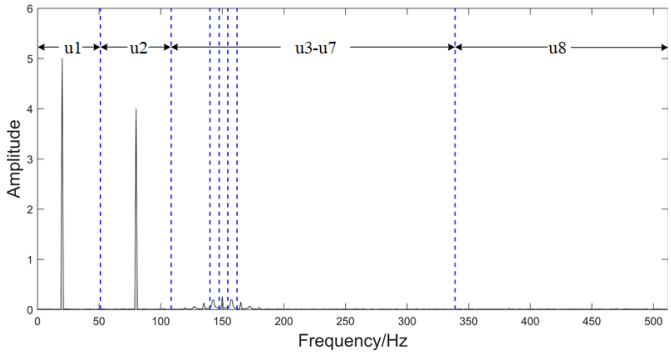

Fig. 7. Analysis result of spectrum, when $K = 8$.

TABLE II
ENERGY ENTROPY OF EACH MODE

Modes	u1	u2	u3	u4
EE_i	0.3028	0.3675	0.0075	0.0128
Modes	u5	u6	u7	u8
EE_i	0.0109	0.0125	0.0071	0.0016

C. Identification of Chatter Frequency Band Based on FFT

To determine whether the frequency band includes these chatter frequencies, the spectrum of the raw signal is solved, which can reflect the frequency bands of all modes.

In Fig. 7, the modes are named u1, u2, u3, u4, u5, u6, u7, and u8. As is seen, the frequency of u1 mainly focuses on 20 Hz, which is the low frequency of x_1; the frequency of u2 mainly focuses on 80 Hz, which is the high frequency of x_2; the frequencies of u3–u7 mainly focus on the frequency band [100 Hz, 200 Hz], which is the simulation chatter frequencies of x_3; the frequencies of u8 represent the frequency of the added white noise x_4.

D. Energy Entropy and Error Analysis of the Reconstructed Signal

For finding out the best mode, energy entropy is calculated and the results are shown in Table II.

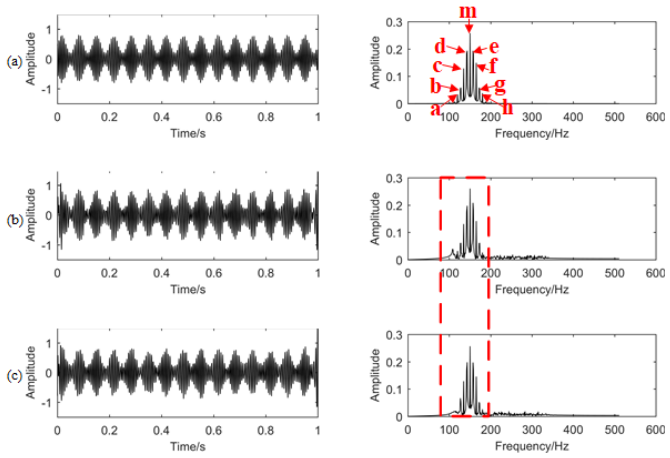

Fig. 8. Raw chatter signal, other two reconstruction signals, and its FFT. (a) Raw signal x_3. (b) Reconstruction signal u_{rc} under $K = 8$. (c) u_3 under $K = 4$.

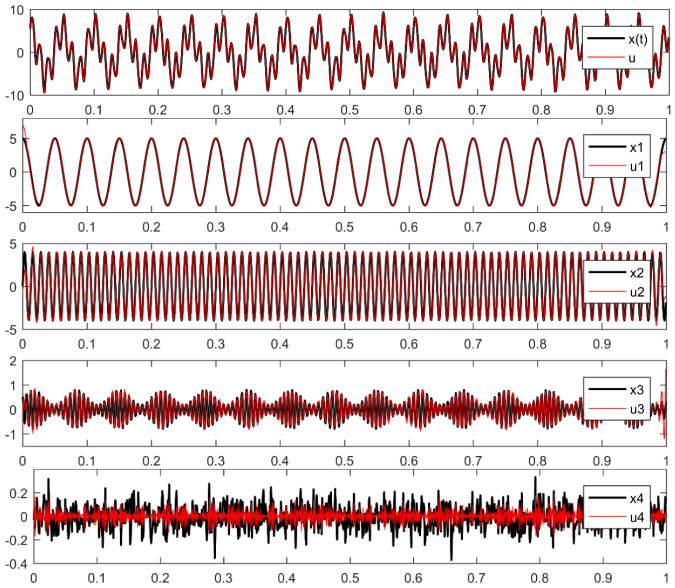

Fig. 9. Comparison between the raw signals and the decomposed results.

In the above table, u1 and u2 have the bigger energy entropy than other modes. They represent the low-frequency and high-frequency components, respectively. Otherwise, from the analysis result of FFT, u3–u7 are found to be chatter bands. However, their energy entropies are significantly lower than those of u1 and u2, which show that the energy in the chatter frequency band is not higher than that in the low frequency and the high frequency.

After finding out the best modes representing the chatter information, the reconstruction signal is composed of u3–u7, and is called u_{rc}. The spectrum of the raw signals x_3 and u_{rc} can be seen in Fig. 8(a) and (b).

Since the simulation signal contains four components, K is assumed as 4. In order to show the proposed method's validity, the result under $K = 4$ is shown in Fig. 8(c) and u_3 is the third mode after decomposing the signal. The comparison between the raw signal and the result under $K = 4$ is shown in Fig. 9.

TABLE III
AMPLITUDE OF CHATTER FREQUENCIES IN THREE SIGNALS

Frequency	a/120Hz	b/128Hz	c/135Hz	d/143Hz
raw signal	0.0330	0.0581	0.1279	0.1931
u_{rc}	0.0315	0.0612	0.1298	0.1968
u_3	0.0157	0.0632	0.1292	0.1959
Frequency	e/157Hz	f/165Hz	g/172Hz	h/180Hz
raw signal	0.1931	0.1485	0.0581	0.0377
u_{rc}	0.2077	0.1408	0.0599	0.0257
u_3	0.2071	0.1438	0.0616	0.0281

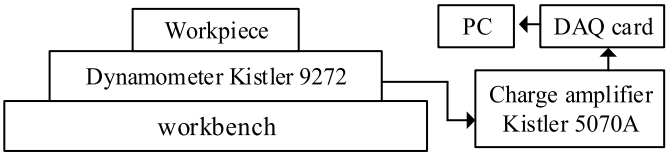

Fig. 10. Measurement setup test block diagram.

The reconstruction signal is described in terms of u, which is the sum of four modes. It is seen from Fig. 9 that u, u1, u2, and u3 are almost the same as x, x1, x2, and x3. Since x4 is the white noise, u4 is significantly different from x4. Additionally, x3 simulates the chatter frequencies, so u3 and its FFT are shown in Fig. 8(c). Compared with u_3, u_{rc} has little difference from the raw signal. In Fig. 8(a), eight chatter frequencies can be found, so the amplitude of chatter frequencies in three signals is compared in Table III.

After comparing the amplitude of eight chatter frequencies of u_{rc} and u_3 with that of the raw signal x_3, the effect of u_{rc} is obviously better than that of u_3 on the whole.

VI. EXPERIMENTAL VERIFICATION

A. Experimental Setup

The experiments were finished in a CNC milling machine, which used a two-fluted flat end milling tool whose diameter and helix angle are 10 mm and 35°, respectively. In addition, the material of workpieces is the aluminum alloy 6061.

During this, cutting force signals were used for chatter detection. The devices in the experiment include a dynamometer and a charge amplifier. The sampling frequency is 12 000 Hz and the whole milling process is in the dry state. The measurement setup is shown in Fig. 10. Even though a small amount of workpiece material is removed during milling, it has little influence on the modal parameters of the milling system, which barely influence the effectiveness of this chatter detection method.

B. Results and Discussion

1) Frequency Analysis: In cutting tests, cutting conditions are shown in Table IV. Through spectrum analysis, FFT can easily detect the chatter frequency. The cutting force signal under three conditions and their spectrum are shown in Fig. 11.

As seen in Fig. 11, the range of cutting force in test 1 is [−25, 25], the range of force in test 2 is [−40, 40], and the range of force in test 3 is [−120, 120]. Therefore,

TABLE IV
CUTTING CONDITIONS

Group	Test	Milling type	Radial depth of cut (mm)	Axial depth of cut (mm)	Cutting speed (mm/min)	Spindle speed (r/min)
	1	Down	slot	0.4	198	6600
	2	Down	slot	0.6	198	6600
	3	Down	slot	0.7	198	6600

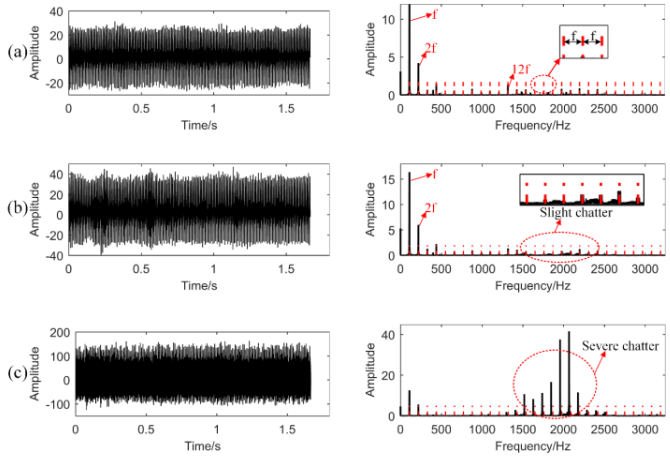

Fig. 11. Cutting force signal and its spectrum. (a) Stable condition under test 1. (b) Slight chatter under test 2. (c) Severe chatter under test 3.

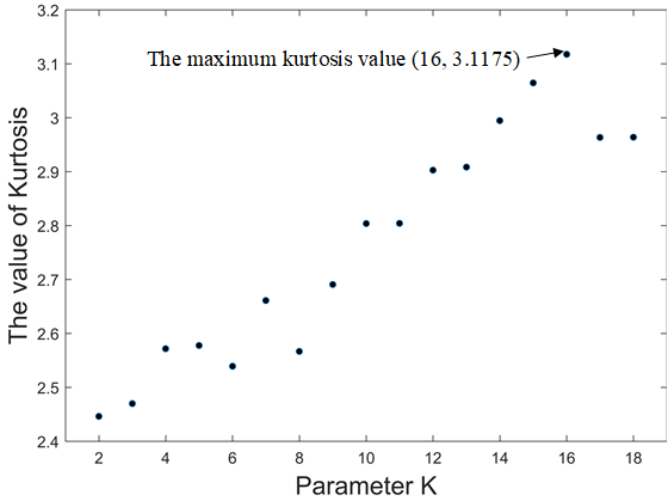

Fig. 12. 2-D graph of kurtosis under all possible K.

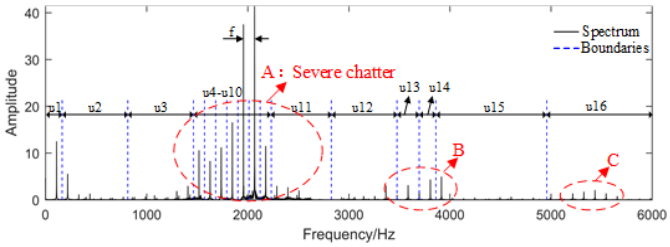

Fig. 13. Analysis result of the spectrum when $K = 16$.

the cutting force increases with the increase of the axial depth. The spindle speed is 6600 r/min, which means its rotation frequency is 110 Hz and the tooth passing frequency is 220 Hz. The chatter frequency is defined by the frequency which is different from the rotation frequency and its multiple frequencies. In order to find out the chatter frequency, the rotation frequency and its multiple frequencies are described by the red dotted lines in Fig. 11. As is seen, the frequencies of test 1 mainly concentrated on the rotation frequency and its multiple frequencies, so the milling process is stable; the frequencies of test 2 are still mainly concentrated on the rotation frequency and its multiple frequencies, but some frequencies have been transferred to other frequencies, as shown in the red circle in Fig. 11(b), so the cutting condition causes slight chatter; the frequencies of test 3 are not concentrated on the rotation frequency and its multiple ones, but mainly in the frequency of the natural frequency (2068 Hz) in Fig. 11(c), so the chatter is severe.

2) Analysis Based on the Combination of MEWT and Energy Entropy: The height of the FFT peak indicates the severity of chatter. However, FFT can only detect chatter after milling and cannot locate the time of chatter simultaneously. Chatter detection requires real-time feedback of the processing status and gives the corresponding warning of chatter. Therefore, an automatic chatter detection method based on MEWT and the energy entropy is proposed. First, the method is to solve the kurtosis of the test 3's cutting force. It is similar to the parameter setting of the simulation signal. The limit value δ is set to 0.05% empirically and $K_{\max} = 18$ is calculated with this δ. The step of K, T_K, is set to 1. The kurtosis of all K is shown in Fig. 12.

As seen from Fig. 12, when $K = 16$, the maximum kurtosis is 3.1175. Then, the signal is decomposed by MEWT under this K. To determine whether these 16 modes belong to the chatter frequency band, FFT is carried out on them, as shown in Fig. 13.

In Fig. 13, u1–u3 are the frequency bands including the rotation frequency and its multiple frequencies. u4–u16 are the frequency bands including the chatter frequencies. In addition, the chatter frequency is obviously modulated by the rotation frequency f. Besides, circle A in Fig. 13 shows that the chatter frequencies resulted from the natural frequency (2068 Hz), and the chatter frequencies in circles B and C might result from the higher natural frequency of this milling system.

In order to find the optimal component indicating chatter, the energy entropy of u1–u16 is solved, as shown in Fig. 14.

When the cutting process is stable, the energy is mainly concentrated on u1, u2, u3, and u11, which is consistent with the rotation frequency and its multiple frequencies included in u1, u2, and u3. But the energy entropy transfers when slight chatter occurs. The energy entropy of u7, u9, and u10 increased with the chatter, and the energy is mainly concentrated on u1, u2, u3, u9, u10, and u11 when there is slight chatter. With severe chatter, the energy is mainly concentrated on the chatter bands, such as u9, u8, u7, u6, and u10. The energy entropies of u8 and u9 have become the largest two values. After considering the changing pattern,

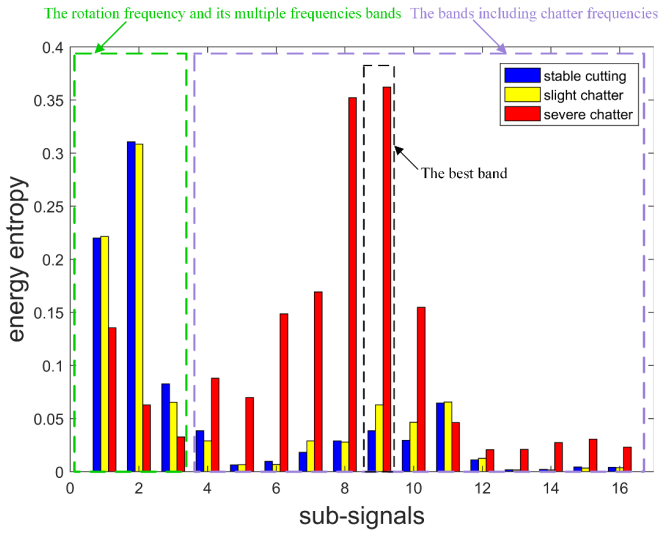

Fig. 14. Energy entropy of each subsignal when $K = 16$.

TABLE V
ENERGY ENTROPY OF THE OVERALL SIGNAL IN THREE TESTS

Cutting condition	Stable (test 1)	Slight chatter (test 2)	Severe chatter (test 3)
Energy entropy	0.8710	0.8921	1.7451

the energy entropy of u9 can be seen as the best chatter indicator, since it has an obvious rate of change.

The energy entropy of u9 is only 0.0385 in stable cutting (test1), 0.0628 in slight chatter (test 2), and 0.3622 in severe chatter (test 3). The rate of growth of u9's energy entropy is 63.12% from stable to slight chatter, and it is 476.75% from the slight chatter to severe chatter. So, u9 will be the selected indicator of chatter, which have excellent sensitivity to different chatter states. The energy entropy of the overall signal is calculated to show the better performance of this method. The energy entropy of the overall signal in three different tests is shown in Table V.

In the table, we can see that the rate of growth is only 2.42% from the stable to slight chatter, so the growth rate of u9 in the same process is roughly 26 times that of the overall signal. Besides, the rate is only 95.6% from the slight to severe chatter, which is a fifth of the rate in the proposed method. In a word, certain subsignal u9's sensitivity is higher than the overall signal's and u9 can be the chatter indicator with its wonderful sensitivity performance.

To show the advantage of this detection, the computation time was recorded. In this experiment, the proposed detection algorithm took 18.92 s to run in MATLAB. Though the speed is obviously slow than that of FFT, it can help us to determine slight chatter at an early stage, which can help the engineers to stop the milling process, adjust the cutting parameters, and reduce the rejection rate.

VII. CONCLUSION

This article proposes the MEWT which utilizes the MFs and 1-D Otsu to segment the spectrum better. The local maxima distribution plane of MFs is utilized to find out the optimal threshold of MFs, which considers those useful dominant peaks in the spectrum. The simulation signal is processed by EWT and MEWT, and the results show that MEWT has better boundary segmentation. MEWT will be helpful in fault diagnosis fields because of its advanced peaks retention effect and boundary division.

Then, in the chatter detection method, an automatic selection of the decomposed parameter K using biggest kurtosis is proposed and it improves its previous empirical selection. Additionally, the calculated energy entropy of each subsignal helps detect chatter frequency bands and choose the optimal chatter monitor indicator. The simulation signal and experimental signals including chatter frequencies have been analyzed for verifying the effectiveness of the novel chatter detection method with strong sensitivity to slight chatter, which can monitor the chatter at an early stage and reduce the rate of defective products.

However, the optimization of δ should be our next step work, because the maximum possible $K_{\max}$ is determined by the empirical value δ at present. Besides, although the speed of the algorithm in this chatter detection method cannot be compared with the speed of the FFT, the proposed detection method can confirm chatter earlier with strong sensitivity to chatter, which is of great significance for the practical milling process.

REFERENCES

[1] Y. Altintas, G. Stepan, D. Merdol, and Z. Dombovari, "Chatter stability of milling in frequency and discrete time domain," *CIRP J. Manuf. Sci. Technol.*, vol. 1, no. 1, pp. 35–44, 2008.
[2] G. Quintana and J. Ciurana, "Chatter in machining processes: A review," *Int. J. Mach. Tools Manuf.*, vol. 51, no. 5, pp. 363–376, 2011.
[3] M. Uekita and Y. Takaya, "Tool condition monitoring technique for deep-hole drilling of large components based on chatter identification in time–frequency domain," *Measurement*, vol. 103, pp. 199–207, Jun. 2017.
[4] M. Wang, L. Gao, and Y. Zheng, "Prediction of regenerative chatter in the high-speed vertical milling of thin-walled workpiece made of titanium alloy," vol. 72, nos. 5–8, pp. 707–716, 2014.
[5] R. Rafal, L. Pawel, K. Krzysztof, K. Bogdan, and W. Jerzy, "Chatter identification methods on the basis of time series measured during titanium superalloy milling," *Int. J. Mech. Sci.*, vol. 99, pp. 196–207, Aug. 2015.
[6] H. Moradi, G. Vossoughi, M. Behzad, and M. R. Movahhedy, "Vibration absorber design to suppress regenerative chatter in nonlinear milling process: Application for machining of cantilever plates," *Appl. Math. Model.*, vol. 39, no. 2, pp. 600–620, 2015.
[7] R. Teti, K. Jemielniak, G. O. Donnell, and D. Dornfeld, "Advanced monitoring of machining operations," *CIRP Ann.*, vol. 59, no. 2, pp. 717–739, 2010.
[8] M. Siddhpura and R. Paurobally, "A review of chatter vibration research in turning," *Int. J. Mach. Tools Manuf.*, vol. 61, pp. 27–47, Oct. 2012.
[9] A. Baus, E. Govekar, F. Klocke, and I. Grabec, "Automatic chatter detection in grinding," *Int. J. Mach. Tools Manuf.*, vol. 43, no. 14, pp. 1397–1403, 2003.
[10] D. Pérez-Canales, L. Vela-Martínez, J. C. Jáuregui-Correa, and J. Alvarez-Ramirez, "Analysis of the entropy randomness index for machining chatter detection," *Int. J. Mach. Tools Manuf.*, vol. 62, pp. 39–45, Nov. 2012.
[11] C. Liu, L. Zhu, and C. Ni, "The chatter identification in end milling based on combining EMD and WPD," *Int. J. Adv. Manuf. Technol.*, vol. 91, nos. 9–12, pp. 3339–3348, 2017.
[12] J. C. Jauregui-correa, E. Rodriguez, J. Alvarez-ramirez, and L. Vela-Martínez, "Using detrended fluctuation analysis to monitor chattering in cutter tool machines," *Int. J. Mach. Tools Manuf.*, vol. 50, no. 7, pp. 651–657, 2010.

[13] M. Lamraoui, M. Thomas, and M. E. Badaoui, "Cyclostationarity approach for monitoring chatter and tool wear in high speed milling," *Mech. Syst. Signal Process.*, vol. 44, nos. 1–2, pp. 177–198, 2014.
[14] H. Liu, Q. Chen, B. Li, X. Mao, K. Mao, and F. Peng, "On-line chatter detection using servo motor current signal in turning," *Sci. China Technol. Sci.*, vol. 54, no. 12, pp. 3119–3129, 2011.
[15] Z. Yang, H. Liu, B. Li, and X. Liu, "Recognition of chatter in boring operations using spindle motor current," in *Proc. Int. Conf. Trans., Mech., Elect. Eng.*, Dec. 2011, pp. 2158–2161.
[16] H. Cao, Y. Yue, X. Chen, and X. Zhang, "Chatter detection in milling process based on synchrosqueezing transform of sound signals," *Int. J. Adv. Manuf. Technol.*, vol. 89, no. 9–12, pp. 2747–2755, 2017.
[17] K. M. Hynynen *et al.*, "Chatter detection in turning processes using coherence of acceleration and audio signals," *J. Manuf. Sci. Eng.*, vol. 136, no. 4, pp. 2–5, Aug. 2014.
[18] P. Potočnik, I. Bric, E. Govekar, and T. Thaler, "Chatter detection in band sawing based on discriminant analysis of sound features," *Appl. Acoust.*, vol. 77, pp. 114–121, Mar. 2014.
[19] I. N. Tansel, M. Li, M. Demetgul, K. Bickraj, B. Kaya, and B. Ozcelik, "Detecting chatter and estimating wear from the torque of end milling signals by using Index Based Reasoner (IBR)," vol. 58, nos. 1–4, pp. 109–118, 2012.
[20] O. González-Brambila, E. Rubio, J. C. Jáuregui, and G. Herrera-Ruiz, "Chattering detection in cylindrical grinding processes using the wavelet transform," *Int. J. Mach. Tools Manuf.*, vol. 46, no. 15, pp. 1934–1938, 2006.
[21] Y. Yu and C. Junsheng, "A roller bearing fault diagnosis method based on EMD energy entropy and ANN," *J. Sound Vib.*, vol. 294, nos. 1–2, pp. 269–277, 2006.
[22] F. A. Khasawneh and E. Munch, "Chatter detection in turning using persistent homology," *Mech. Syst. Signal Process.*, vols. 70–71, pp. 527–541, Mar. 2016.
[23] Z. Lv, B. Tang, Y. Zhou, and C. Zhou, "A novel method for mechanical fault diagnosis based on variational mode decomposition and multikernel support vector machine," *Shock Vib.*, vol. 2016, 2016, Art. no. 3196465.
[24] D. A. Axinte, N. Gindy, K. Fox, and I. Unanue, "Process monitoring to assist the workpiece surface quality in machining," *Int. J. Mach. Tools Manuf.*, vol. 44, no. 10, pp. 1091–1108, 2004.
[25] E. Kuljanic, G. Totis, and M. Sortino, "Development of an intelligent multisensor chatter detection system in milling," *Mech. Syst. Signal Process.*, vol. 23, no. 5, pp. 1704–1718, 2009.
[26] J. P. Amezquita-Sanchez and H. Adeli, "Signal processing techniques for vibration-based health monitoring of smart structures," *Arch. Comput. Methods Eng.*, vol. 23, no. 1, pp. 1–15, 2016.
[27] H. Cao, K. Zhou, and X. Chen, "Chatter identification in end milling process based on EEMD and nonlinear dimensionless indicators," *Int. J. Mach. Tools Manuf.*, vol. 92, pp. 52–59, May 2015.
[28] C. Zhang, B. Li, B. Chen, H. Cao, Y. Zi, and Z. He, "Weak fault signature extraction of rotating machinery using flexible analytic wavelet transform," *Mech. Syst. Signal Process.*, vols. 64–65, pp. 162–187, Dec. 2015.
[29] S. Karam and R. Teti, "Wavelet transform feature extraction for chip form recognition during carbon steel turning," *Procedia CIRP*, vol. 12, pp. 97–102, 2013.
[30] J. Gilles, "Empirical wavelet transform," *IEEE Trans. Signal Process.*, vol. 61, no. 16, pp. 3999–4010, Aug. 2013.
[31] Z. Zhang, H. Li, G. Meng, X. Tu, and C. Cheng, "Chatter detection in milling process based on the energy entropy of VMD and WPD," *Int. J. Mach. Tools Manuf.*, vol. 108, pp. 106–112, Sep. 2016.
[32] C. Liu, L. Zhu, and C. Ni, "Chatter detection in milling process based on VMD and energy entropy," *Mech. Syst. Signal Process.*, vol. 105, pp. 169–182, May 2018.
[33] W. Xi, L. Bai, M. Hui, and Q. Wu, "A novel rolling bearing fault detect method based on empirical wavelet transform," in *Proc. 13th IEEE Conf. Ind. Electron. Appl.*, May 2018, pp. 2764–2768.
[34] Y. Sun, C. Zhuang, and Z. Xiong, "A scale factor-based interpolated DFT for chatter frequency estimation," *IEEE Trans. Instrum. Meas.*, vol. 64, no. 10, pp. 2666–2678, Oct. 2015.
[35] Y. Hu, F. Li, H. Li, and C. Liu, "An enhanced empirical wavelet transform for noisy and non-stationary signal processing," *Digit. Signal Process.*, vol. 60, pp. 220–229, Jan. 2017.
[36] N. Otsu, "A threshold selection method from gray-level histograms," *IEEE Trans. Syst., Man, Cybern., Syst.*, vol. SMC-9, no. 1, pp. 62–66, Jan. 1979.

Qi Zhang received the B.S. degree in mechanical engineering from Hunan University, Changsha, China, in 2017. He is currently pursuing the master's degree in mechanical engineering with Shanghai Jiao Tong University, Shanghai, China.

He is currently with the State Key Laboratory of Mechanical System and Vibration, Shanghai Jiao Tong University. His current research interest includes signal processing and machine health diagnosis.

Xiaotong Tu received the B.Eng. degree in mechanical engineering from Northeastern University, Shenyang, China, in 2014. He is currently pursuing the Ph.D. degree in mechanical engineering with Shanghai Jiao Tong University, Shanghai, China.

He is currently with the State Key Laboratory of Mechanical System and Vibration, Shanghai Jiao Tong University. His research interests are mainly in rotating machinery fault diagnosis and machine learning.

Fucai Li received the B.Eng. and Ph.D. degrees in mechanical engineering from Xi'an Jiao Tong University, Xi'an, China, in 1998 and 2003, respectively.

He is currently a Professor with Shanghai Jiao Tong University, Shanghai, China. His current research interests include structural health monitoring, fault diagnosis for mechanical systems, sensing technology, and digital signal processing.

Yue Hu received the B.Eng. degree from the Huazhong University of Science and Technology, Wuhan, China, in 2013. He is currently pursuing the Ph.D. degree in mechanical engineering with Shanghai Jiao Tong University, Shanghai, China.

His research interests are mainly in rotating machinery failure diagnosis and digital signal processing.